ACCOUNTS of chemical research

Computational Chemistry Meets Cultural Heritage: Challenges and Perspectives

SIMONA FANTACCI,* ANNA AMAT, AND ANTONIO SGAMELLOTTI

Istituto di Scienze e Tecnologie Molecolari del CNR (CNR-ISTM) and Dipartimento di Chimica via Elce di Sotto, Università degli Studi di Perugia, 01623-Perugia, Italy

RECEIVED ON JANUARY 13, 2010

CONSPECTUS

Chemistry is central to addressing topics of interest in the cultural heritage field, offering particular insight into the nature and composition of the original materials, the degradation processes that have occurred over the years, and the attendant physical and chemical changes. On the one hand, the chemical characterization of the constituting materials allows researchers to unravel the rich information enclosed in a work of art, providing insight into the manufacturing techniques and revealing aspects of artistic, chronological, historical, and sociocultural significance. On the other hand, despite the recognized contribution of computational chemistry in many branches of materials science, this tool has only recently been applied to cultural heritage, largely because of the inherent complexity of art materials.

In this Account, we present a brief overview of the available computational methods, classified on the basis of accuracy level and dimension of the system to be simulated. Among the discussed methodologies, density functional theory (DFT) and time-dependent DFT represent a good compromise between accuracy and computational cost, allowing researchers to model the structural, electronic, and spectroscopic properties of complex extended systems in condensed phase.

We then discuss the results of recent research devoted to the computer simulation of prototypical systems in cultural heritage, namely, indigo and Maya Blue, weld and weld lake, and the pigment minium (red lead). These studies provide insight into the basic interactions underlying the materials properties and, in some cases, permit the assignment of the material composition. We discuss properties of interest in the cultural heritage field, ranging from structural geometries and acid-base properties to IR−Raman vibrational spectra and UV−vis absorption−emission spectra (including excited-state deactivation pathways). We particularly highlight how computational chemistry applications in cultural heritage can complement experimental investigations by establishing or rationalizing structure−property relations of the fundamental artwork components. These insights allow researchers to understand the interdependence of such components and eventually the composition of the artwork materials.

As a perspective, we aim to extend the simulations to systems of increasing complexity that are similar to the realistic materials encountered in works of art. A challenge is the computational investigation of materials degradation and their associated reactive pathways; here the possible initial components, intermediates, final materials, and various deterioration mechanisms must all be simulated.

Introduction

The link between art and science has always been strong since artists have always had a deep knowledge of the employed materials properties and have often experimented with recipes that mixed natural ingredients to obtain new materials or color nuances. Nevertheless, art and chemistry have often been considered very distant fields, and only recently chemistry has achieved a conscious role in artwork restoration and conservation within cultural heritage. Thus, along with restorers, art historians, and museum curators,

Published on the Web 04/29/2010 www.pubs.acs.org/acr
10.1021/ar100012b

chemists have investigated art materials and the basic processes ruling their properties. The topics of interest within the chemistry of cultural heritage are related to an in depth comprehension of (i) the nature and composition of original materials, (ii) the physical and chemical changes that occurred over the years, affecting both the materials composition and their chromatic properties, and (iii) the factors responsible for the artwork modifications (oxidation processes, acid or basic agents, light irradiation, humidity, etc.). As a matter of fact, the contribution of chemical and physical sciences on the characterization of the materials can be crucial in unraveling the rich information enclosed in a work of art, information that may reveal aspects of historical and artistic significance and can also be used for restoration and conservation purposes. In this respect, the development of new analytical methodologies and noninvasive spectroscopic techniques and the design of portable monitoring equipment have made of analytical and physical chemistry a keystone for cultural heritage.[1]

Computational chemistry has gained great consideration in a variety of fields from the pharmaceutical industry to the development of functional materials. The accuracy reached in simulating the properties of complex extended systems, along with the development of efficient algorithms and high-performance computers, makes computational chemistry a valuable interpretative and predictive tool that allows both the comprehension and rationalization of experimental data and the modeling of new materials. Despite the recognized contribution of computational chemistry, this technique has only very recently been applied to the cultural heritage field. While this is certainly because of the recent approach of chemistry to cultural heritage, a major reason underlying the distance between computational chemistry and artwork is also that art materials show an inherent complexity, which in many cases is very difficult to model and sometimes even to capture. This is in turn because the investigated systems are in some cases not well-defined and are continuously changing throughout the times in an unmonitored way.

A main goal of computational chemistry application to the cultural heritage field is to provide a complementary approach to experimental investigations in determining structure−property relations of the fundamental artwork components, thus allowing researchers to understand the interdependencies of such components in the investigated system and eventually the composition of artwork materials.[2]

We present selected recent applications, in which computational chemistry tools have been used to simulate the electronic and spectroscopic properties of cultural heritage materials (indigo[3,4] and Maya Blue,[5,6] weld[7−9] and weld lake,[10] and minium[4]) providing insight into the basic interactions underlying the material properties.

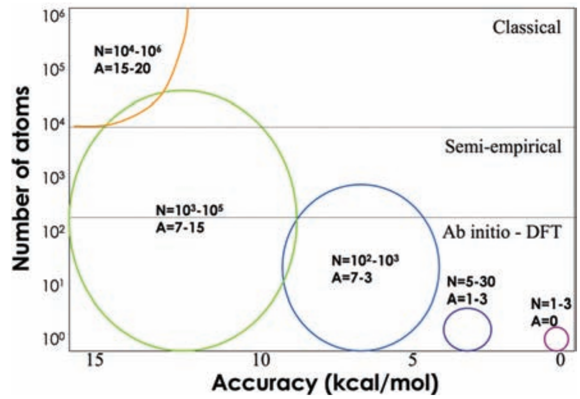

FIGURE 1. Schematic representation of the number of atoms vs accuracy (kcal/mol) of computational methods.

Methodology Overview

Computational chemistry includes a collection of methods that can be classified in terms of the method accuracy against the computational cost involved in solving the associated equations. Since the computational cost in terms of computer resources usually scales as some power >1 of the systems dimensions, a trade-off between the simulated system dimensions and the method accuracy needs to be achieved. We report in Figure 1 a schematic representation of the scale/accuracy hierarchy of computational methods. In this framework, quantum mechanics represents the highest level, allowing us in principle to calculate *exactly* the wave function and therefore all the properties of any ensemble of atoms. In practice, approximate solutions to the many-electron Schrödinger equation need to be devised, giving rise to the family of so-called *ab initio* methods, in which the quantum mechanical equations are solved exactly but using an approximate form for the wave function. The basis of *ab initio* tools is the Hartree−Fock method, from which electron correlation can be introduced by perturbation theory (MPn, $n = 2, 3, 4$), coupled cluster (CC), or multiconfigurational (CASSCF/CASPT2) approaches. A different approach is represented by density functional theory (DFT), in which the exact one-electron density, rather than many-electron wave function, is pursued. Here an approximate exchange−correlation (xc) functional of the electron density is devised, which contains the quantum mechanical electron−electron interactions. DFT usually offers a favorable computational scaling, at least comparable to the simplest Hartree−Fock *ab initio* method, yet retaining a considerable accuracy, which makes DFT the method of choice for most applications. Moreover, the recently developed time-dependent DFT extension (TDDFT)[11] gives access to accurate excited-state properties at a reasonable computational cost. In both *ab initio* and DFT frameworks, environmental effects can be included by exploiting the computational convenience of continuum solvation models, in which the solvent is described as a structureless polarizable dielectric medium.[12,13]

Systems larger than a few hundred atoms cannot be routinely treated by *ab initio*/DFT methods, so semiempirical techniques (INDO, MNDO, AM1, ZINDO, etc.) can be employed in which an approximate description of electron–electron interactions is used to simplify and speed the solution of the quantum mechanical equations. Very recently a tight-binding approximation to DFT (so-called DFT-B) has emerged as a powerful approach to the description of extended molecular and periodic systems.[14,15] Beyond semiempirical methods, the electronic description of the investigated systems is lost, and atomic interactions are described by model potentials (e.g., Lennard-Jones) within the framework of classical mechanics. The associated computational overhead is drastically diminished at the expense of a substantial loss of accuracy and generality. An alternative approach is that of hybrid methods (QM/MM), which integrate an "active site" described at a high-level (e.g., quantum mechanical) and a "surrounding system" described by a lower level (e.g., classical mechanics).[16]

All the methods described give access to a "static" picture of the investigated system, allowing calculation of equilibrium geometries and related properties. A powerful simulation tool that allows one to go beyond this static picture is molecular dynamics (MD), which describes the time evolution of an ensemble of particles under a given interatomic potential. MD simulations require the repeated (10^4–10^5) evaluation of the interatomic potential and forces, thus solving the associated classical equations of motion. To circumvent the computational cost associated with the iterative evaluation of the interatomic potential, Car and Parrinello devised a classical MD tool[17] in which the interatomic potential is derived on the fly from DFT, thus combining the power of MD and the accuracy of DFT.

Indigo and Maya Blue

Indigo, Figure 2, is one of the most ancient natural dyes; its history starts in India in the pre-Vedic period where *Indigofera tinctoria* L. was its more common source.[18] Indigo is also the fundamental chromophore constituting the Maya Blue pigment, Figure 2, produced by the ancient Mayan civilization in pre-Columbian America. Two characteristics of Maya Blue are the bright hue and the stability to chemical and biodegradation, which are most likely related to its inorganic–organic hybrid nature.[19] The indigo dye is bound into the palygorskite mineral, even though the nature of the indigo–palygorskite binding modes is an open debate and in literature controversial information are reported.[20−22]

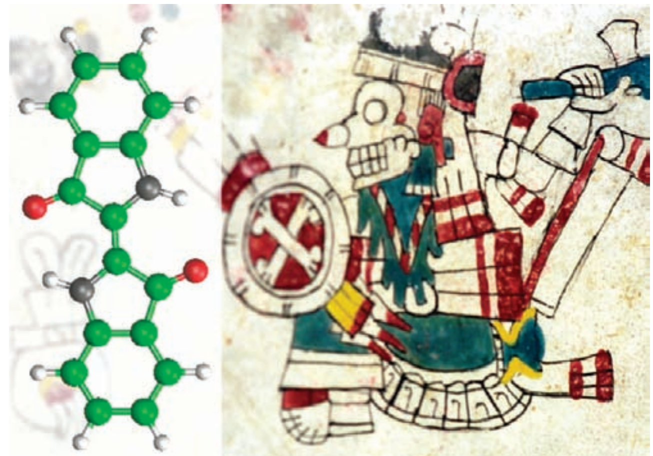

FIGURE 2. Indigo molecular structure and a typical Maya Blue decoration (prehispanic Cospi Codex, Biblioteca Universitaria, Bologna, Italy).

Due to its relevance, the indigo dye has been widely investigated both experimentally and theoretically, with target properties being vibrational (both IR and Raman)[23,24] and UV–vis spectra.[3,25]

The indigo UV–vis absorption spectrum was simulated employing both correlated multiconfigurational[25] and TDDFT[3] methods. TDDFT calculations in solution (PCM) based on hybrid functionals turned out to be extremely accurate upon using large basis sets (within 0.02 eV), compared with experimental data. These calculations were able to quantitatively reproduce the bathochromism of the indigo absorption spectrum observed in solvents of increasing polarity compared with gas phase, which was assigned to the increased contribution of charge-separated excited states in solvents of higher polarity.[3]

Experimental evidence of indigo aggregation in apolar solvents has also been detected,[26] characterized by the appearance of a new band around 700 nm at high indigo concentrations, Figure 3. Based on the interactions occurring in the solid state,[3] we simulated hydrogen-bonded indigo dimers and trimers, optimizing their structure by DFT in chloroform solution and performing TDDFT excited-state calculations in solution on the optimized structures.[4] The indigo molecules in the dimer and trimer optimized structures (Figure 3) are not coplanar (dihedral angles of ~30°) and show a rather strong intermolecular hydrogen bonding interaction between the carbonyl oxygen and the nitrogen-bound hydrogen, amounting to 16.7 and 26.7 kcal/mol for the dimer and trimer, respectively, suggesting the possible formation of

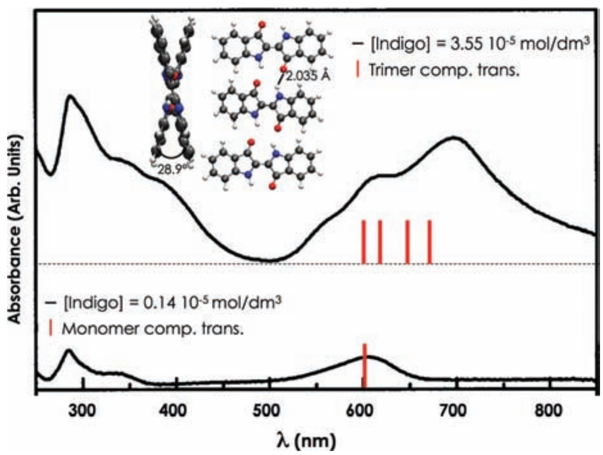

FIGURE 3. Optimized indigo trimer structure. Experimental absorption spectra in chloroform solutions at different concentrations[26] with the computed TDDFT excitation energies for the monomer (lower) and the trimer aggregate (upper) (B3LYP/6-31G*/PCM calculations).[4]

extended aggregates in apolar solvents, in agreement with the experimental hypothesis.[27]

Inspection of the TDDFT eigenvectors suggests that the 0.17−0.19 eV shift calculated from the monomer to the dimer and trimer spectrum (605 vs 660 and 670 nm, respectively) originated from intermolecular interactions giving rise to excitonic splitting of the excited states.[4]

Hydrogen-bonding host−guest interactions between the indigo dye and the inorganic matrix or inner zeolitic water molecules[22] in palygorskyte seem also to be responsible of the peculiar behavior of Maya Blue, including the color change from blue of solid state indigo to turquoise-greenish of Maya Blue observed upon thermal treatment.[28] According to molecular dynamics simulations,[6] corroborated by experimental evidence,[29] indigo can favorably insert into the inner cavities of palygorskyte, being stabilized by either hydrogen bonding or interactions of the carbonyl group with cations (Mg, Al) constituting the inorganic matrix. Furthermore, dehydroindigo can also be found within palygorskyte as a consequence of the thermal treatment.[20]

Recent Car−Parrinello simulations combined with TDDFT excited-state calculations performed by Tilocca and Fois have confirmed the host−guest interactions underlying the stability of Maya Blue.[5] The simulations included an extended model of palygorskyte with inserted indigo, Figure 4, or dehydroindigo. By extracting representative models of the interaction between the organic dyes and the inorganic matrix, the authors were able to associate the optical response exhibited by Maya Blue compared with solid-state indigo to interactions between the carbonyl groups of the organic dyes and Al(III) cations of the inorganic matrix.

Weld and Weld Lake: A Yellow Organic Pigment

Lakes represent an interesting class of colored materials used in antiquity. Even though lakes are also known as organic pigments, they are metal−organic systems obtained by adding metal salts to dyestuffs solutions. Depending on the combined natural dyes and metal cations (i.e., Al(III), Fe(II) and Sn(II)), a wide selection of lake pigments were prepared, which were highly prized for their rich color and transparency even though more prone to degradation with respect to the inorganic pigments. As a consequence, topics of interest within painting conservation are related to an in depth comprehension of the nature and composition of lakes.[30] Weld, extracted from *Reseda luteola* L., is one of the oldest natural dyes known in Europe, and its use is traced back to the beginning of the Christian Era.[31,32] According to ancient treatises, weld lake was prepared by adding potash alum (aluminum potassium double sulfate) to an alkaline solution of the dyestuff until neutrality was achieved. After precipitation of the Al−dye complex together with hydrated alumina, the resulting yellow organic pigment was filtered, washed with distilled water, dried, and finely ground in a mortar.[30]

Weld optical properties are due to the apigenin (Ap) and luteolin (Lu) hydroxyflavonoids contained in the plant, see molecular structures in Figure 5, which are approximately in 1:9 ratio. Recently, weld lake has been prepared at the Scientific Department of the National Gallery (London) according to the recipes reported in ancient treatises.[30] The absorption spectra of this yellow lake exhibits a broad band with a maximum at ca. 410 and a pronounced shoulder at 380 nm.

To investigate weld and weld lake, a spectrophotometric and fluorimetric study of Ap and Lu before and upon Al(III) addition was performed.[33] The maxima of the lowest energy absorption band of Ap and Lu measured in MeOH−water (1/2, v/v) were found at 337 and 348 nm, respectively, Figure 6.

In methanol, Ap was found to exhibit a weak excitation-dependent double emission ($\phi_f = 4 \times 10^{-4}$), with a maximum at 430 nm and a shoulder at 534 nm ($\lambda_{exc} = 300$ nm), while only the 534 nm feature was retrieved when the system was excited at 357 nm, see Figure 7. For luteolin, no emission was detectable.[33]

Moreover, both the hydroxyflavonoids exhibit a marked acidochromism, which produces an absorption red shift when the solution pH is increased.[33]

The spectroscopic changes upon additions of Al(III) ions to methanol solutions of Ap and Lu have also been investigated,

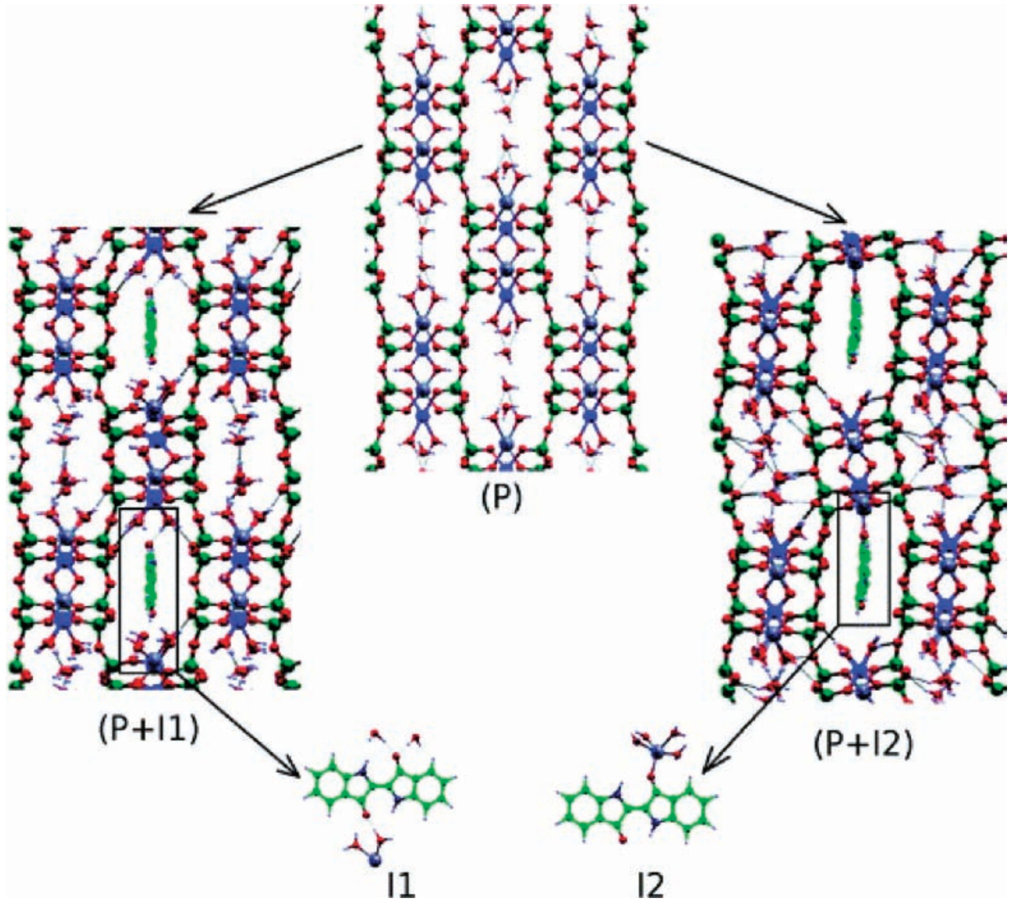

FIGURE 4. Optimized structure of palygorskite (P) and of two specific host−guest interactions: (i) hydrogen-bonding interaction with zeolitic waters (P + I1); (ii) interaction with Mg^{2+} or Al^{3+} (P+I2) or (P+I3), respectively. The small models, I1, I2, and I3, representative of specific palygorskite−indigo interactions, were extracted for TDDFT calculations.[5] Reprinted with permission from ref 5. Copyright 2009 American Chemical Society.

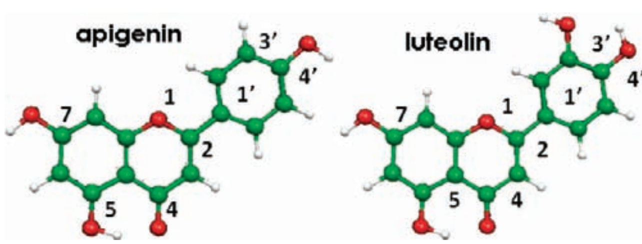

FIGURE 5. Optimized geometry of apigenin and luteolin hydroxyflavonoids constituting weld (B3LYP/6-31G**/PCM calculations).[8,9]

finding that (i) in the Ap case, the Al^{3+} concentration increase implies the appearance of a band at 382 nm, which is maintained at high Al^{3+} concentration, and (ii) in the Lu case, three different limit Al^{3+} concentrations are identified (8×10^{-6}, 5×10^{-5}, and 3×10^{-4} mol/dm^3), which can probably be associated with three different complexation steps, see Figure 9.

Absorption and Emission of Apigenin and Luteolin. We simulated the absorption spectra of Ap and Lu in water and methanol, finding for both flavonoids at different levels of theory an excellent agreement with the experimental data in energy and band shape,[9] Figure 6. Moreover, from analysis of the TDDFT eigenvectors, we were able to characterize the transitions responsible for the main absorption bands in terms of the involved molecular orbitals, finding that the low-energy absorption band at 337 (348) nm for Ap (Lu) is composed of two rather separate transitions of $\pi-\pi^*$ character computed at 352 and 321 (361 and 331) nm, the latter showing a partial charge transfer character, see Figure 7. We demonstrated that the inclusion of solvation effects is mandatory for an accurate description of the optical properties of these natural dyes,[9] as previously observed for inorganic dyes.[34]

To investigate the Ap emission process, TDDFT optimization of the lowest excited state has been performed, finding an excited-state optimized structure characterized by an intramolecular proton transfer, ESIPT.[9] To trace an approximate proton transfer pathway, we have computed the potential energy curves on S_0 and S_1 as a function of the O_5H distance. Our results suggest that upon Ap excitation to the Franck−Condon (FC) point, a first relaxation process occurs

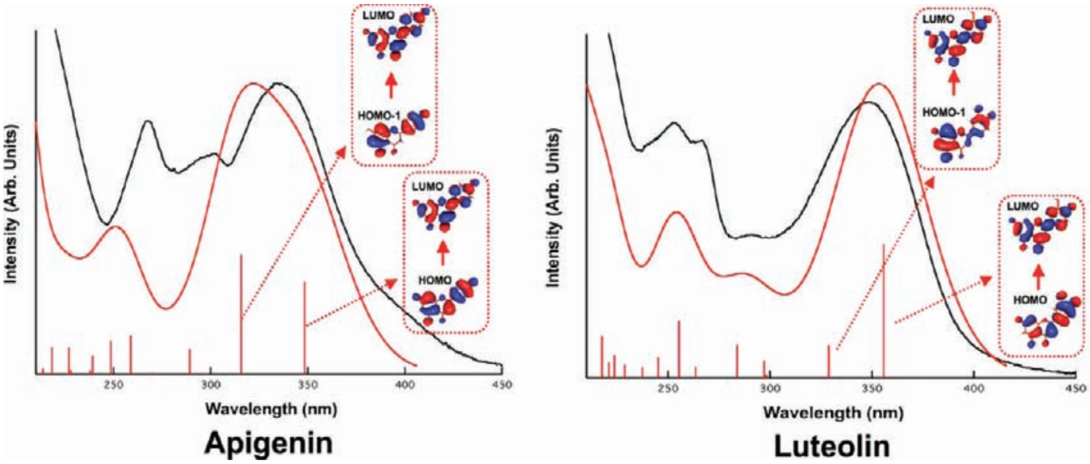

FIGURE 6. Comparison between the experimental[33] and computed spectra of apigenin and luteolin, together with selected molecular orbitals isodensity plots (B3LYP/6-31G**/PCM TDDFT calculations).[9]

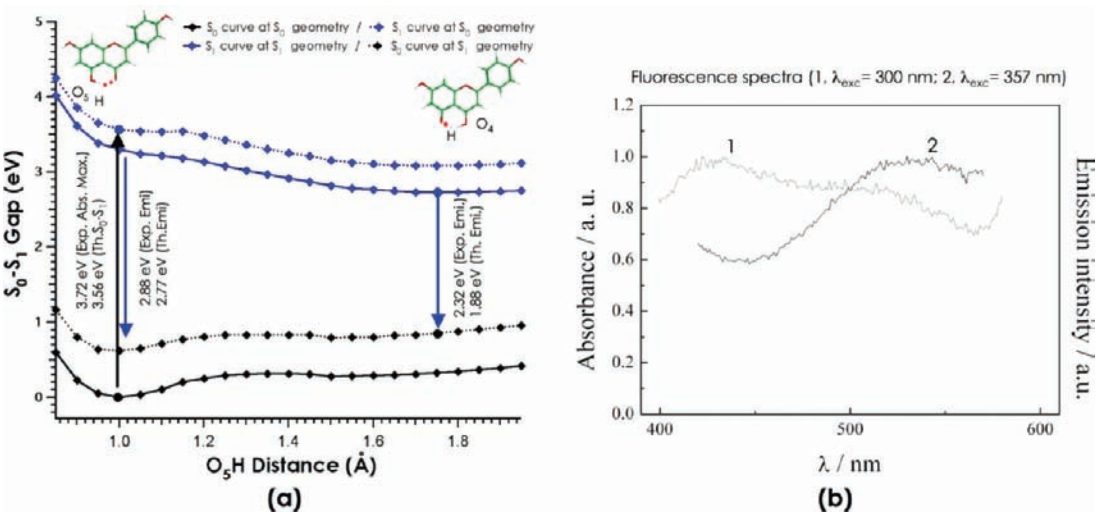

FIGURE 7. (a) Apigenin proton transfer potential energy curve at different O_5H fixed distances for the ground (S_0) and first excited (S_1) state (B3LYP/6-31G**/PCM calculations).[9] (b) Experimental fluorescence spectra.[33]

through a planarization of the molecule. From the FC region, the excited-state energy decreases rapidly to a flat region corresponding to the ESIPT minimum structure. From this excited-state minimum, we calculate an emission energy of 1.9 eV to be compared with the experimental value of 2.3 eV. Although no local minimum structure has been calculated by TDDFT in the flat energy region around the FC point, the presence of an O_5-bound excited-state minimum calculated by CIS suggests that the fluorescence experimentally measured at 2.9 eV, calculated at 2.8 eV, might be due to emission from an excited-state structure that has not yet undergone the ESIPT process.

Acid–Base Properties: pK_a Assignment and Absorption Spectra. As for many organic dyes, the absorption and fluorescence spectra of Ap and Lu markedly depend on the pH.[33] Since both flavonoids show several hydroxyl groups characterized by similar pK_a values, it is crucial, also for conservation purposes, to accurately identify the acidity order of the Ap and Lu deprotonation sites. The only related experimental information is represented by the study by Wolfbeis et al.[35] on methoxy-substituted Lu, which allowed the unambiguous pK_a assignments. As a benchmark for pK_a calculations, we therefore evaluated the pK_a for all the possible methyl ether luteolin derivatives.[8] The pK_a calculations were performed according to the procedure detailed in ref 36, demonstrating that deprotonation in position 4′ leads to an increase of conjugation and an overestimation of the monodeprotonated species stability that lowers the pK_a providing the wrong acidity order, Figure 8. We therefore performed additional MP2 calculations,[7,8] reproducing the correct acidity order and computing pK_a′s in good agreement with the experimental values, with maximum deviations of 1.5 pK units.

We thus extended this methodological procedure to the pK_a calculation of the deprotonation sites of both luteolin and

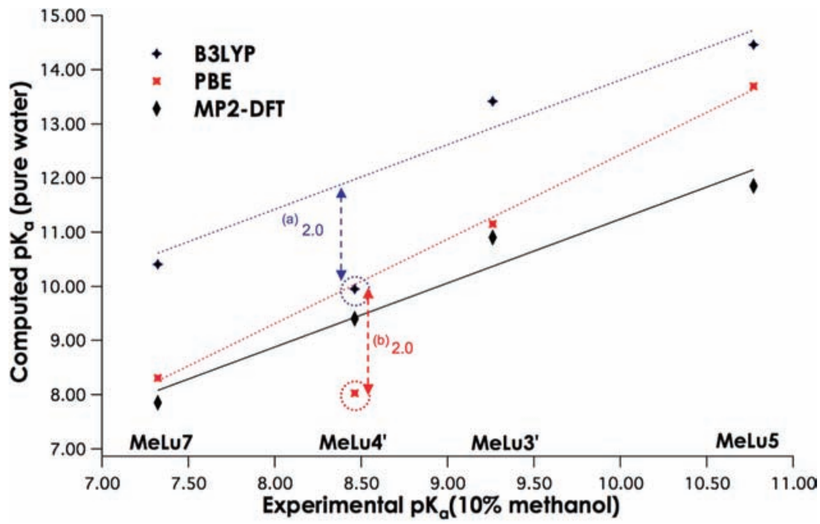

FIGURE 8. Experimental pK_a's in water/methanol vs computed pK_a's in water and at different levels of theory. Straight line in black is the linear fitting for all the four MP2-PBE values. Dotted lines are the linear fitting for MeLu5, MeLu7, and MeLu3′ pK_a's computed with PBE (red) and B3LYP(blue). Values a and b are the MeLu4′ deviations from the corresponding correlation for B3LYP and PBE data, respectively.[8]

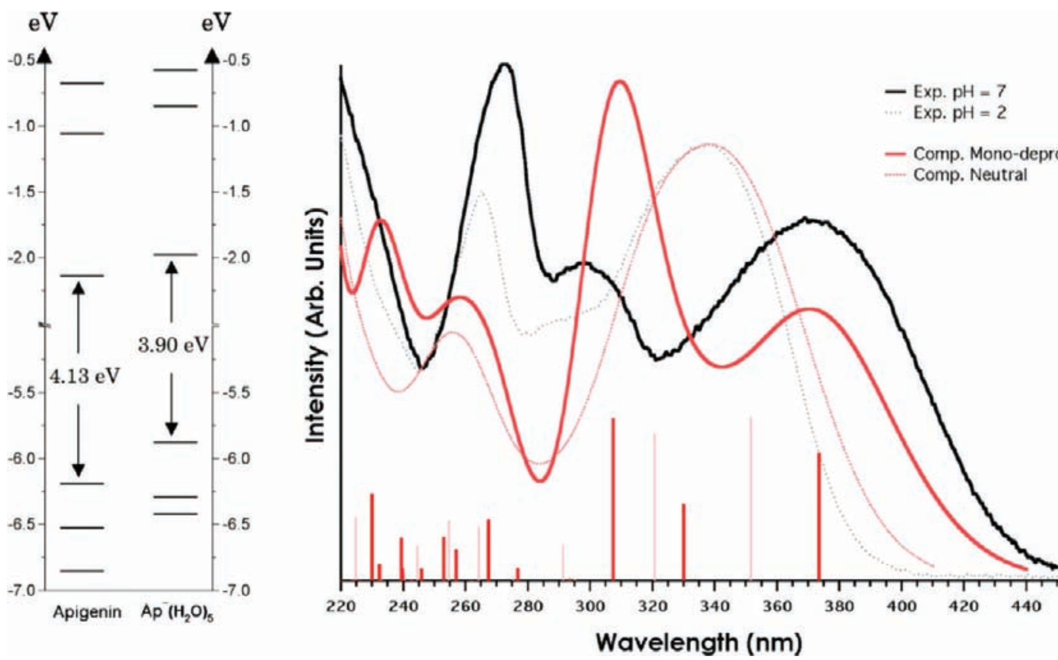

FIGURE 9. (a) Molecular orbitals levels of neutral and monodeprotonated apigenin with five explicit water molecules. (b) Apigenin experimental spectra at pH = 2 and 7 (black) from ref 33 compared with computed spectra of the neutral and monodeprotonated apigenin cluster with five explicit water molecules (red) (B3LYP/6-31+G**/PCM calculations).[9]

apigenin. According to our MP2 results, for apigenin we computed pK_a values of 7.44, 8.66, and 11.60 for positions 7, 4′, and 5, respectively. These results allowed us to undertake the study of the spectral modifications with increasing pH, by relating the experimental absorption spectrum of the monodeprotonated species to the deprotonated apigenin in position 7. The red shift experimentally observed upon deprotonation is qualitatively retrieved when a few explicit water molecules are added to the system, to take into account specific solute−solvent interactions. In the present case, the deprotonation results mainly in stabilizing the HOMO and decreasing the HOMO−LUMO gap compared with the neutral case, see Figure 9.

Aluminum Complexation of Apigenin and Luteolin. To elucidate the composition of the weld lake, all the possible $Al(H_2O)_n$−Ap/Lu complexes were investigated (n is the number of water molecules to reach the Al^{3+} octhaedral arrangement) by optimizing their equilibrium geometries, computing their formation Gibbs free energies (ΔG), and eventually simulating their UV−vis absorption spectra.[10] The comparison

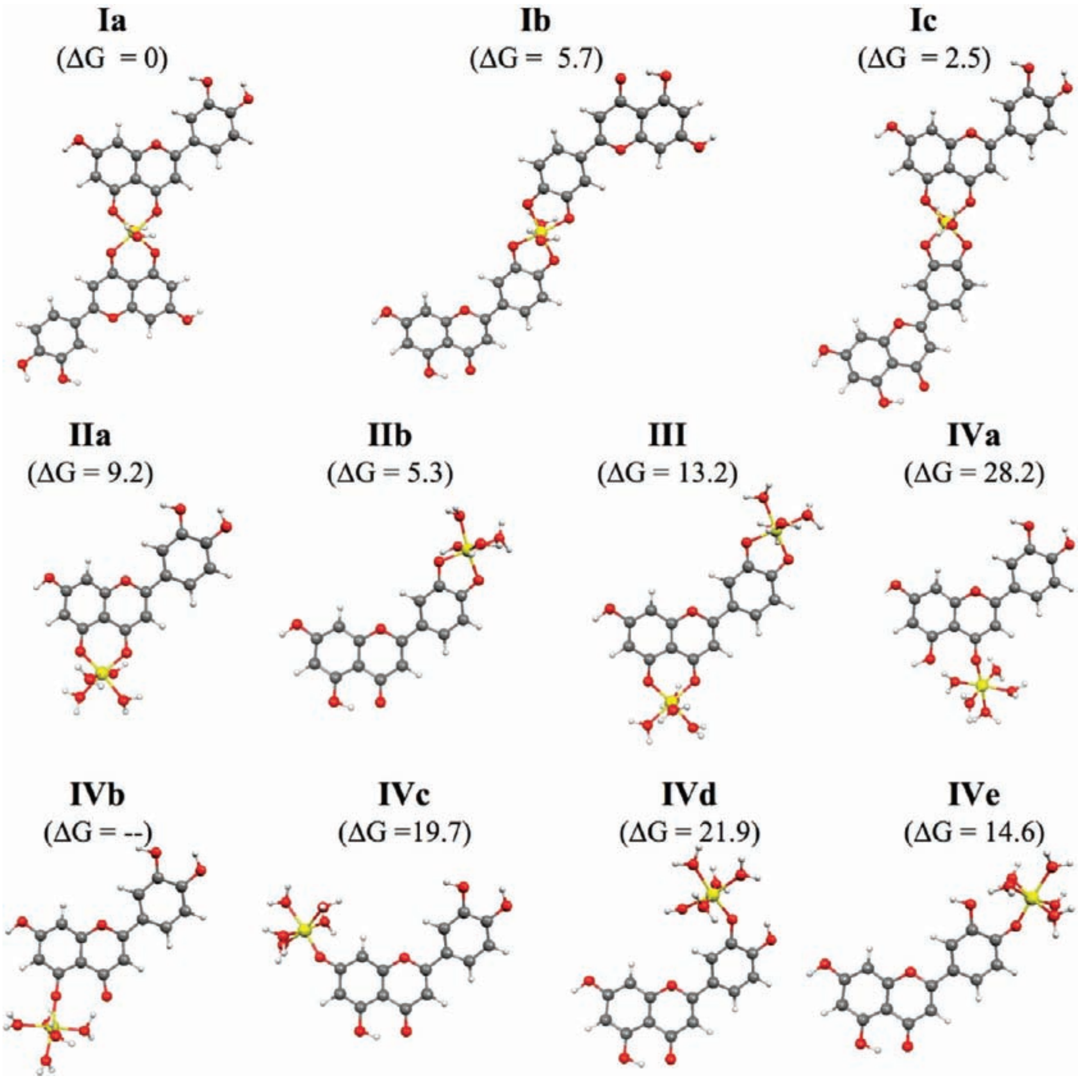

FIGURE 10. Optimized geometries of Al−Lu complexes and related formation Gibbs free energies (Δ*G*) in kcal/mol (B3LYP/6-31G**/PCM calculations).[10]

between the computed absorption spectra of the Al−hydroxyflavonoid complexes and the experimental ones corresponding to various relative [Al^{3+}] and [Ap]/[Lu] concentrations was used, along with formation free energies, to discriminate among the possible chelation modes and stoichiometries. Given the composition of weld, we assume that weld lake will be preferentially related to the formation of Al−Lu complexes. In principle, the luteolin 3′,4′-dyhydroxyl and 5-hydroxy-4-keto functionalities can act as bidentate chelating groups, thus opening a scenario of six bidentate complexes, see Figure 10: (i) pseudocarboxyl- and catechol-binding sites with Al/Lu 1:2 (**Ia** and **Ib**); (ii) same but with Al/Lu 1:1 stoichiometry (**IIa** and **IIb**); (iii) a 1:2 Al/Lu complex involving the two different sites of each luteolin (**Ic**); and (iv) a binuclear 2:1 Al/Lu complex involving both carboxylic and cathecolic functionalities of the same luteolin (**III**). Alongside the bidentate complexation modes, the five Al-monodentate complexes involving all the hydroxylic and the carbonylic groups have been also taken into account (see Figure 10, **IVa**−**IVe** complexes).

The calculated formation free energies have highlighted a marked preference for the bidentate chelating modes, but due to the small energy differences among bidentate complexes, we were not able to reach a definitive assignment. We thus resorted to comparison between calculated and experimental UV−vis absorption spectra. The best match between theory and experiment at [Al^{3+}] = 8×10^{-6} mol/dm^3 is found for the absorption spectrum of complex **Ia**, Figure 11, even though the absorption band intensities are inverted with respect to the experiment. The absorption spectrum at [Al^{3+}] = 5×10^{-5} mol/dm^3 nicely agrees with that computed for **IIa**, which shows a 1:1 Al/Lu stoichiometry, Figure 11. The computed spectrum of the binuclear complex **III** is in excellent

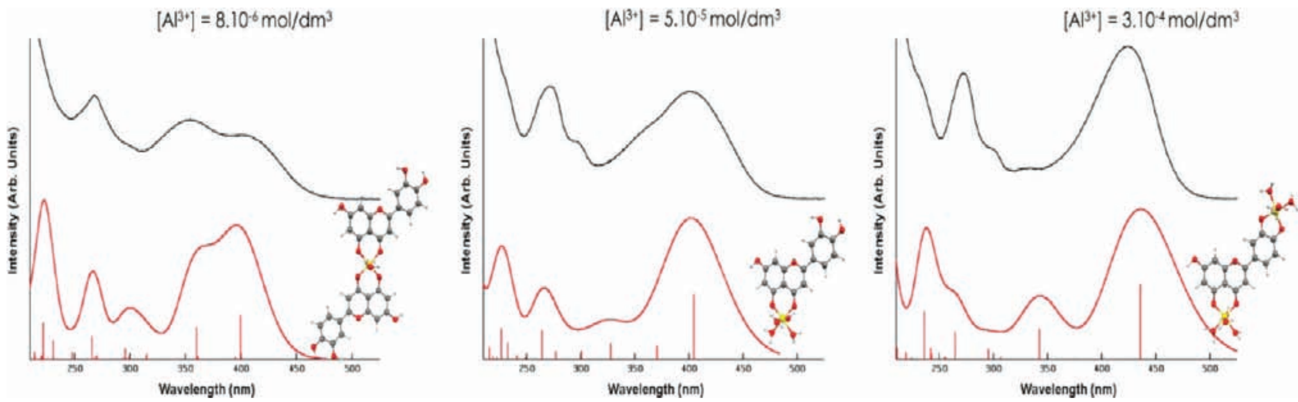

FIGURE 11. Al−Lu complexes **Ia**, **IIa**, and **III** computed (red line) vs experimental (black line) spectra from ref 33 at 8×10^{-6} (I), 5×10^{-5} (II), and 3×10^{-4} (III) mol/dm^3 [Al^{3+}] (B3LYP/6-31G**/PCM TDDFT calculations).[10]

agreement with the experimental absorption spectrum at high [Al^{3+}], both in terms of spectral shape and absorption energy, Figure 11.

As a general observation, the lowest absorption bands of the complexes **Ia** and **IIa** appear broad and with some band substructure: indeed, our calculations reveal that these are originated by two or three transitions, while in the binuclear complex the lowest computed absorption band is the result of only one intense transition, consistent with the experiment, see Figure 11.

We found Al chelation to stabilize the lowest HOMOs, therefore producing the red-shift of the lowest absorption band of complexes **Ia** and **IIa**.

We can thus exploit the calculated results on luteolin complexation to speculate upon the composition of weld lake. As mentioned above, this lake was prepared by adding potash alum to an alkaline solution of weld; upon alum addition to water, $Al(H_2O)_6^{3+}$ is formed. This trivalent cation in alkaline solution undergoes a series of rapid hydrolytic reactions to form soluble monomeric and polymeric species, as well as the $Al(OH)_3$ in a solid phase. The dye molecules may be involved in the precipitation of hydrate alumina as coprecipitated Al complexes or being adsorbed on the surface of the amorphous solid.[10,30] This solid is present in different polymorphs, which have in common the same layer, $Al(OH)_6$ distorted octahedra sharing the same edge, but arranged in different motifs.[37] The UV−vis reflectance spectrum of weld lake exhibits a strong absorption in the visible spectral region with a single maximum at 410 nm. This band is very similar to that observed for luteolin at intermediate [Al^{3+}] and therefore related to the **IIa** complex. We might argue that luteolin is adsorbed on the $Al(OH)_3$ surface via a bidentate Al/Lu 1:1 mode involving only the favored 4-keto-5-hydroxy chelating site.

As a concluding remark to this section, we can extend the applied procedure to the identification of putative decomposition products, occurring with the materials aging, by jointly calculating their thermodynamic stability and optical properties.

Minium, a Red Inorganic Pigment

Lead-based pigments have been used since antiquity due to their bright colors and high covering power.[38,39] Red and yellow lead oxides have been considered by art historians to be the earliest artificial pigments and have been widely used in artwork such as paintings, manuscripts, and ceramics.[39,40] The various lead oxides can present different stoichiometry ratios and composition, due to not well-defined syntheses in terms of involved reagents and experimental conditions.[40]

Among the lead-based pigments, minium, also known as red lead, has probably been employed since the time of the development of lead metallurgy in both China and the Near East.[39] The preparation of minium from lead was known in Greek and Roman times, where it was prepared by calcination of litharge (tetragonal PbO) or lead white ($PbCO_3$). In the ancient and medieval periods, it was extensively used as a pigment in the production of bright manuscripts, giving its name to the miniature.

The use of theoretical methods to model the spectroscopic properties of hypothesized and well-defined structures can provide insight into the unknown pigment compositions and structures through the comparison with experiment, allowing discrimination among various possible oxides. In particular, here we focus on the simulation of the minium Raman spectrum as a benchmark for further investigation of other possible oxides with variable composition.

Minium has a Pb_3O_4 formula, in which lead assumes two different oxidation states, Pb(II) and Pb(IV), which occupy dif-

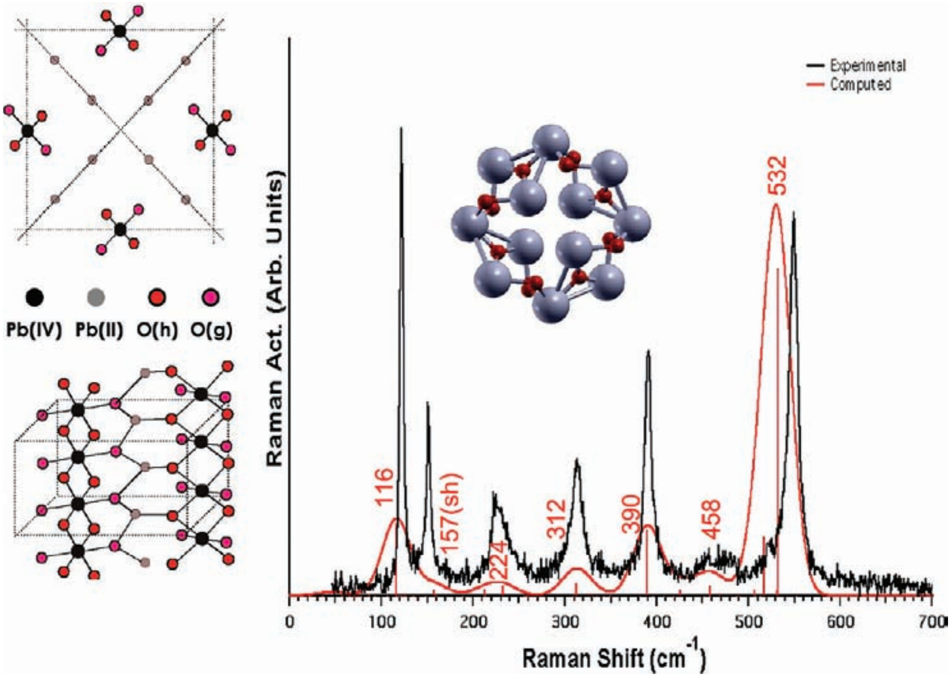

FIGURE 12. (left) Pb_3O_4 tetragonal structure, characterized by the $P4_2/mbc$-D^{13}_{4h} group with cell axes $a = b = 8.811$ Å and $c = 6.563$ Å[41] (right) Computed Pb_3O_4 Raman spectrum at the crystallographic cell dimensions vs experimental scattering excited at $\lambda_{exc} = 785$ nm. The crystal unit cell of minium (inset of Raman spectrum) shows four Pb(IV), octahedrally coordinated to six oxygens, four in the h position and two in the g position and eight Pb(II), coordinated to three oxygen atoms, one in the h position and two in the g position, in an asymmetric pyramid arrangement. For further computational details see ref 48.

ferent structural sites. Pb(IV)−O arrange in chains of octahedra sharing opposite edges, while these chains are linked by the Pb(II) centers characterized by a pyramidal arrangement, Figure 12.

Several experimental studies employing Raman spectroscopy have been performed on minium.[42−45] This spectroscopic technique has been used to evaluate the mixture compositions in ancient pigment samples[43] and combined with scanning electron microscopy to investigate the deterioration mechanisms of minium.[42]

Previous DFT investigations performed on Pb_3O_4 have assigned the material band structure,[46] revising earlier data obtained at the semiempirical level.[47]

We have optimized the structure of Pb_3O_4 solid and simulated its Raman spectrum within a DFT-based periodic-boundary conditions approach.[48]

The calculated bond distances and angles are in excellent agreement with the crystallographic data, with maximum deviations within 0.08 Å.[4] The Pb_3O_4 simulated Raman spectrum is reported in Figure 12. All the main features of the experimental Raman spectrum are well reproduced by our calculations. Bands at higher Raman shifts are mainly due to the O displacements and, except for the bands computed at 532 and 390 cm^{-1}, are exclusive either of the h or the g oxygen, see Figures 12 and 13. Similarly, the computed transitions are divided into strictly parallel or perpendicular displacements along the crystal *c* axis, except for the bands at 517 and 213 cm^{-1}, which exhibit displacements of g oxygens along each axis.

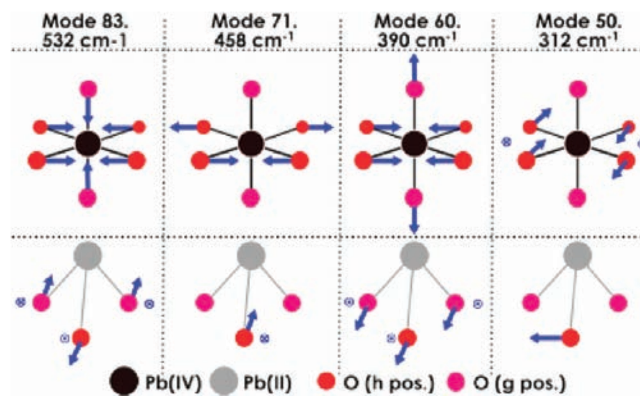

FIGURE 13. Main Pb_3O_4 vibrational modes active in Raman.

In the low wavenumber region, a single band is computed at 116 cm^{-1} with a shoulder at 157 cm^{-1} related to Pb displacements. The *c*-axis perpendicular displacements of the Pb(II) atoms are responsible for the strong transition computed at 116 cm^{-1}, while the weak 157 cm^{-1} transition is related to both Pb(IV) and Pb(II) displacements perpendicular and parallel to *c*-axis, respectively. Some of the principal modes of the Raman spectra are depicted in Figure 13 and discussed hereafter.

Concerning modes involving atoms in the coordination sphere of Pb(IV) centers, we find a predominance of scissoring modes with the O(h) oxygens. Vibrations at 532 and 390 cm^{-1} also involve symmetric stretching with the O(g) oxygens, while at 312 cm^{-1}, we find only Pb(IV)−O(h) rocking modes. Concerning modes involving Pb(II), vibrations at 532 and 390 cm^{-1} show Pb(II)O(g) wagging modes that are out and in phase with the Pb(II)O(h), respectively. On the other hand vibrations at 458 and 312 cm^{-1} involve only O(h) pendulum-like displacements that are perpendicular and parallel to the Pb(II)O(g) plane, respectively.

In summary, our calculations allows us to accurately reproduce and assign the experimental spectroscopic features of solid inorganic pigments, thus paving the way for further investigations on crystalline or amorphous materials and on their decomposition pathways, by exploiting structure/property relations on selected candidate structures, in analogy to diagnostic tools employed experimentally.

Conclusions and Outlook

We reported on few applications of computational chemistry to materials of interest in the field of cultural heritage. The integration of various computational levels into a unique protocol allows researchers to tackle systems of increasing complexity at various levels of accuracy. Structure−properties relationships have been established with great accuracy, highlighting how *ab initio* and DFT/TDDFT calculations, including continuum solvation models and molecular dynamics, can support and complement the experimental information obtained from analytical and spectroscopic techniques. Based on these results on prototypical model systems, a first goal to be accomplished is to extend the simulation of vibrational and optical spectra to systems of increasing complexity, matching eventually the realistic materials encountered in works of art. The inherent complexity of such materials will require researchers to devise new methodologies and strategies integrating methods of variable accuracy levels into a unique multiscale computational protocol.

A challenge in the field of conservation science is the investigation of the materials degradation and their associated reactive pathways. In this framework, computational chemistry can assume a central role in understanding the various deterioration mechanisms and evolution of art materials through time, by the joint calculation of the thermodynamic stability and spectroscopic properties of selected candidate structures.

We acknowledge F. De Angelis, G. B. Brunetti, C. Miliani, A. Romani, and S. Scandolo for helpful discussions.

BIOGRAPHICAL INFORMATION

Simona Fantacci received a Ph.D. in Chemistry from the University of Perugia (Italy) in 1998. Since 2001, she has been a research scientist at the CNR-ISTM, Perugia. She was research associate at Princeton University (USA) in 2002−2003. Her research interests reside in the investigation of the electronic and optical properties of complex systems by DFT/TDDFT methods.

Anna Amat is a postdoctoral researcher at the University of Perugia working on the application of theoretical methods to cultural heritage.

Antonio Sgamellotti is Professor of Inorganic Chemistry at the University of Perugia, President of the Center of Excellence SMAArt (Scientific Methodologies applied to Archaeology and Art), and author of more than 300 scientific publications on advanced computational chemistry and on spectroscopic investigations of artwork materials.

FOOTNOTES

*To whom correspondence should be addressed. E-mail: simona@thch.unipg.it.

REFERENCES

1 Janssens, K, van Grieken, R., Eds. *Non-destructive microanalysis of cultural heritage materials*; Elsevier: Amsterdam, 2005; Vol. 42.

2 Wang, M.; Teslova, T.; Xu, F.; Spataru, T.; Lombardi, J. R.; Birke, R. L.; Leona, M. Raman and surface enhanced Raman scattering of 3-hydroxyflavone. *J. Phys. Chem. C* **2007**, *111*, 3038–3043.

3 Jacquemin, D.; Preat, J.; Wathelet, V.; Perpete, E. Substitution and chemical environment effects on the absorption spectrum of indigo. *J. Chem. Phys.* **2006**, *124*, 074104.

4 Amat, A. Materials of interest in the cultural heritage field: theoretical investigations, Ph.D thesis, Università degli Studi di Perugia, Perugia, 2009.

5 Tilocca, A.; Fois, E. The color and stability of Maya blue: TDDFT calculations. *J. Phys. Chem. C* **2009**, *113*, 8683–8687.

6 Fois, E.; Gamba, A.; Tilocca, A. On the unusual stability of Maya blue paint: Molecular dynamics simulations. *Microporous Mesoporous Mater.* **2003**, *57*, 263–272.

7 Amat, A.; De Angelis, F.; Sgamellotti, A.; Fantacci, S. Theoretical investigation of the structural and electronic properties of luteolin, apigenin and their deprotonated species. *J. Mol. Struct. (Theochem)* **2008**, *868*, 12–21.

8 Amat, A.; De Angelis, F.; Sgamellotti, A.; Fantacci, S. Acid-base chemistry of luteolin and its methyl-ether derivatives: A DFT and ab initio investigation. *Chem. Phys. Lett.* **2008**, *462*, 313–317.

9 Amat, A.; Clementi, C.; De Angelis, F.; Sgamellotti, A.; Fantacci, S. Absorption emission of the apigenin and luteolin flavonoids: A TDDFT Investigation. *J. Phys. Chem. A* **2009**, *113*, 15118–15126.

10 Amat, A.; Clementi, C.; Miliani, C.; Romani, A.; Sgamellotti, A.; Fantacci S. Complexation of apigenin and luteolin in weld lake: A DFT/TDDFT investigation. *Phys. Chem. Chem. Phys.*, DOI: 10.1039/B925700D.

11 Casida, M. E., Time-dependent density-functional response theory for molecules. In *Recent Advances in Density Functional Methods, Part I*; Chong, D. P., Ed.; World Scientific: Singapore, 1995; p 155.

12 Klamt, A.; Schüürmann, G. COSMO: A new approach to dielectric screening in solvents with explicit expressions for the screening energy and its gradient. *J. Chem. Soc., Perkin Trans 2* **1993**, 799–805.

13 Cossi, M.; Barone, V.; Cammi, R.; Tomasi, J. Ab initio study of solvated molecules: a new implementation of the polarizable continuum model. *Chem. Phys. Lett.* **1996**, *255*, 327–355.

14 Porezag, D.; Frauenheim, T.; Köhler, T.; Seifert, G.; Kaschner, R. Construction of tight-binding-like potentials on the basis of density-functional theory: Application to carbon. *Phys Rev. B* **1995**, *51*, 12947–12957.

15 Elstner, M.; Porezag, D.; Jungnickel, G.; Elsner, J.; Haugk, M.; Frauenheim, T.; Suhai, S.; Seifert, G. Self-consistent-charge density-functional tight-binding method for simulations of complex materials properties. *Phys Rev. B* **1998**, *58*, 7260–7268.

16 Maseras, F.; Morokuma, K. IMOMM: A New Ab Initio + Molecular Mechanics Geometry Optimization Scheme of Equilibrium Structures and Transition States. *J. Comput. Chem.* **1995**, *16*, 1170–1179.

17 Car, R.; Parrinello, M. Unified approach for molecular-dynamics and density-functional theory. *Phys. Rev. Lett.* **1985**, *55*, 2471–2474.

18 *Artists' Pigments*; Fitzhugh, E.W., Ed.; Oxford University Press: New York, 1997; Vol. 3.

19 van Olphen, H. Maya Blue: A Clay-Organic Pigment. *Science* **1966**, *154*, 645–646.

20 Doménech, A.; Doménech-Carbó, M. T.; Sánchez del Rio, M.; Vázquez de Agredos Pascual, M. L.; Limad, E. Maya Blue as a nanostructured polyfunctional hybrid organic-inorganic material: The need to change paradigms. *New J. Chem.* **2009**, *33*, 2357–2496.

21 Chiari, G.; Giustetto, R.; Druzik,Doehne, E.; Ricchiardi, G. Pre-Columbian nanotechnology: Reconciling the mysteries of the Maya blue pigment. *Appl. Phys. A: Mater. Sci. Process.* **2008**, *90*, 3–7.

22 Giustetto, R.; Llabres i Xamena, F. X.; Ricchiardi, G.; Bordiga, S.; Damin, A.; Gobetto, R.; Chierotti, M. R. Maya Blue: A Computational and Spectroscopic Study. *J. Phys. Chem. B* **2005**, *109*, 19360–19368.

23 del Rio, M. S.; Picquart, M.; Haro-Poniatowski, E.; Elslande, E. V.; Uc, V. H. On the Raman spectrum of Maya blue. *J. Raman Spectrosc.* **2006**, *37*, 1046–1053.

24 Tomkinson, J.; Bacci, M.; Picollo, M.; Colognesi, D. The vibrational spectroscopy of indigo: A reassessment. *Vib. Spectrosc.* **2009**, *50*, 268–276.

25 Serrano Andres, L.; Roos, B. O. A theoretical study of the indigoid dyes and their chromophore. *Chem.—Eur. J.* **1997**, *3*, 717–725.

26 Miliani, C.; Romani, A.; Favaro, G. A spectrophotometric and fluorimetric study of some anthraquinoid and indigoid colorants used in artistic paintings. *Spectrochim. Acta A* **1998**, *54*, 581–588.

27 Cooksey, C. The synthesis and properties of 6-bromoindigo: Indigo blue or Tyran purple? The effect of physical state on the colours of indigo and bromoindigos. *J. Dyes Hist. Archaeol.* **2001**, *16/17*, 97–104.

28 Reinen, D.; Köhl, P.; Müller, C. The nature of the colour centres in Maya blue - the incorporation of organic pigment molecules into the palygorskite lattice. *Z. Anorg. Allg. Chem.* **2004**, *630*, 97–103.

29 Hubbard, B.; Kuang, W.; Moser, A.; Facey, G. A.; Detellier, C. Structural study of Maya blue: Textural, thermal and solid-state multinuclear magnetic resonance characterization of the palygorskite-indigo and sepiolite-indigo. *Clays Clay Miner.* **2003**, *3*, 318–326.

30 Clementi, C.; Doherty, B.; Gentili, P. L.; Miliani, C.; Romani, A.; Brunetti, B. G.; Sgamellotti, A. Vibrational and electronic properties of painting lakes. *Appl. Phys. A: Mater. Sci. Process.* **2008**, *92*, 25–33.

31 Hofenk de Graaff, J. H. *The Colourful Past: Origins, Chemistry and Identification of Natural Dyestuffs*; Achetype Publications: London, 2004.

32 Saunders, D.; Kirby, J. Light-induced colour changes in red and yellow lake pigments. *Natl. Gallery Tech. Bull.* **1994**, *15*, 79–97.

33 Favaro, G.; Clementi, C.; Romani, A.; Vickackaite, V. Acidichromism and ionochromism of Luteolin and Apigenin, the main momponents of the naturally occurring yellow weld: A spectrophotometric and fluorimetric study. *J. Fluoresc.* **2007**, *17*, 707–714.

34 Fantacci, S.; De Angelis, F.; Selloni, A. Absorption spectrum and solvatochromism of the $[Ru(4,4'\text{-}COOH\text{-}2,2'\text{-}bpy)_2(NCS)_2]$ molecular dye by time dependent density functional theory. *J. Am. Chem. Soc.* **2003**, *125*, 4381–4387.

35 Wolfbeis, O. S.; Begum, M.; Geiger, H. The fluorescence properties of luteolines. *Monatsh. Chem.* **1987**, *118*, 1403–1411.

36 Saracino, G. A. A.; Improta, R.; Barone, V. Absolute pK_a determination for carboxylic acids using density functional theory and the polarizable continuum model. *Chem. Phys. Lett.* **2003**, *373*, 411–415.

37 Demichelis, R.; Catti, M.; Dovesi, R. Structure and stability of the $Al(OH)_3$ polymorph doyleite and nordstrandite: A quantum mechanic ab initio study with the crystal06 Code. *J. Phys. Chem. C* **2009**, *113*, 6785–6791.

38 Eastaugh, N.; Walsh, V.; Chaplin, T.; Siddall, R. *Pigment compendium. A Dictionary of Historical Pigments*; Elsevier Butterworth-Heinemann: Oxford, U.K., 2004.

39 *Artists' Pigments*; Fitzhugh, E.W., Ed.; Oxford University Press: Oxford, U.K., 1997; Vol. 1.

40 Rosi, F.; Manuali, V.; Miliani, C.; Brunetti, B. G.; Sgamellotti, A.; Hradil, D.; Grygar, T. Raman scattering features of lead pyroantimonate compounds. Part I: XRD and Raman characterization of Pb2Sb2O7 doped with tin and zinc. *J. Raman Spectrosc.* **2009**, *40*, 107–111.

41 Gavarri, J. R.; Weigel, D. Oxydes de plomb. I. Structure cristalline du minium Pb_3O_4, à température ambiante (293 K). *J. Solid State Chem.* **1975**, *13*, 252–257.

42 Daniilia, S.; Minopoulou, E. A study of smalt and red lead discolouration in *Antiphonitis* wall paintings in Cyprus. *Appl. Phys. A: Mater. Sci. Process.* **2009**, *96*, 701–711.

43 Edwards, H.; Farwell, D. W.; Newton, E. N.; Rull Perez, F. Minium; FT-Raman non-destructive analysis applied to an historical controversy. *Analyst* **1999**, *124*, 1323–1326.

44 Burgio, L.; Clark, R. J. H.; Gibbs, P. J. Pigment identification studies *in situ* of Javanese, Thai, Korean, Chinese and Uighur manuscripts by Raman microscopi. *J. Raman Spectrosc.* **1999**, *30*, 181–184.

45 Eremin, K.; Stenger, J.; Green, M. L. Raman spectroscopy of Japanese artists' materials: The Tale of Genji by Tosa Mitsunobu. *J. Raman Spectrosc.* **2006**, *37*, 1119–1124.

46 Terpstra, H. J.; De Groot, R. A.; Haas, C. The electronic structure of the mixed valence compound Pb_3O_4. *J. Phys. Chem. Solids* **1997**, *58*, 561–566.

47 Evarestov, R. A.; Veryazov, V. A. The electronic structure of crystalline lead oxides. I. Crystal structure and LUC-CNDO calculations. *Phys. Status Solidi (b)* **1991**, *165*, 401–410.

48 Baroni, S.; Dal Corso, A.; de Gironcoli, S.; Giannozzi, P. Quantum ESPRESSO. http://www.pwscf.org.